Deep Ultraviolet Resonance Raman Excitation Enables Explosives Detection

DAVID D. TUSCHEL, ALEKSANDR V. MIKHONIN, BRIAN E. LEMOFF, and SANFORD A. ASHER*

University of Pittsburgh, Department of Chemistry, Pittsburgh, Pennsylvania 15260 (D.D.T., A.V.M., S.A.A.); and West Virginia High Technology Consortium Foundation, 1000 Technology Drive, Fairmont, West Virginia 26554 (B.E.L.)

We measured the 229 nm absolute ultraviolet (UV) Raman cross-sections of the explosives trinitrotoluene (TNT), pentaerythritol tetranitrate (PETN), cyclotrimethylene-trinitramine (RDX), the chemically related nitroamine explosive HMX, and ammonium nitrate in solution. The 229 nm Raman cross-sections are 1000-fold greater than those excited in the near-infrared and visible spectral regions. Deep UV resonance Raman spectroscopy enables detection of explosives at parts-per-billion (ppb) concentrations and may prove useful for stand-off spectroscopic detection of explosives.

Index Headings: **Ultraviolet resonance Raman; Explosives; Energetic materials; Absolute Raman cross-sections; Solution phase; Stand-off detection; Acetonitrile.**

INTRODUCTION

The detection of trace levels of explosives has become more important in the last decade as terrorists have increasingly targeted civilians with improvised explosive devices (IED). Consequently, there is a need for explosives detection by both the military and homeland security organizations. The construction of IEDs varies, and the choice of the method of detection will depend on the form of the device and the environment in which it is to be detected. A variety of techniques based upon chemical identification have been applied for this purpose and these methods are described in the very helpful review by D.S. Moore.[1] Analytical methods explored and developed for IED detection include gas or liquid chromatography, capillary electrophoresis, mass spectrometry, ion mobility spectrometry, infrared absorption spectroscopy, optoacoustic spectroscopy, Raman scattering, fluorescence, chemical reaction colorimetry, and electrochemistry; Moore reviews the strengths and weaknesses of these approaches.

Clearly, some of these methods require sample preparation, and in some cases separations, prior to chemical analysis. Conventional laboratory analysis has proven useful for explosives detection under certain circumstances, e.g., the screening of passenger luggage at airports. In these situations, sample collection by swabbing, separation by chromatography, and identification by benchtop chemical detection methods could readily be performed. In fact, it has been shown that trace amounts of explosives on individuals can be isolated and subsequently identified using confocal micro-Raman spectroscopy.[2,3] Such methods work well when an individual or object has previously been identified as potentially having manufactured an explosive device or is one.

However, some circumstances preclude the use of typical laboratory analytical methods and are best done by remote detection, e.g., an object suspected of being a roadside bomb. Two remote detection methods are laser-induced breakdown spectroscopy (LIBS)[4,5] and Raman spectroscopy.[6–8] Single-shot LIBS spectra with excellent signal-to-noise ratio can readily be obtained at distances of 30 m. However, because LIBS is essentially an atomic emission method it is useful mainly for determining elemental composition; the method lacks clear molecular specificity. In contrast, the Raman band frequencies depend upon chemical bonding in the compounds to be identified. Therefore, remote detection by Raman spectroscopy offers the distinct advantage of chemical specificity and benefits from the ability to generate valid reference Raman spectra under laboratory conditions, against which spectra obtained in the field can be compared.

The major challenge for the use of spontaneous Raman scattering for remote sensing is the inherent weakness of the spontaneous Raman phenomenon and the significant degradation of the Raman spectral signal-to-noise ratios that can result from photoluminescence of the analyte or of the matrix, Nevertheless, there have been numerous attempts to use visible to near-infrared excited Raman for detection of explosives.[6–33] Interference of ambient lighting is a complicating factor for remote detection that is not usually present in laboratory Raman spectral measurements. In spite of the weakness of the Raman effect, several groups have demonstrated the ability to detect Raman scattering from explosives at distances as great as 55 m.[7,8] Carter and co-workers[7] studied the effect of 532 nm excitation spot size, pulse energy, and power density to optimize spectral acquisition and to avoid or minimize sample degradation at stand-off distances of 27 and 50 m. They also studied the utility of detector gating in conjunction with pulsed laser excitation to overcome ambient light interference in the visible region of the spectrum.

Attempts to overcome the inherent weakness of normal Raman scattering and associated visible luminescence has motivated the exploration of deep ultraviolet (UV) resonance Raman spectroscopy for remote detection.[34–39] All explosives show strong deep UV absorption bands that should give rise to increased molecular Raman cross-sections. Furthermore, deep UV excitation below 260 nm in condensed-phase samples avoids fluorescence.[40] In fact, Nagli and co-workers[35] exciting with 248 nm excitation found Raman scattering signals to be 100 to 200 times greater than those obtained with excitation in the visible at 532 nm. Excitation deeper in the UV, further in resonance with the electronic transitions, should give rise to even larger Raman cross-sections. According to Albrecht theory, the Raman intensity will be proportional to the square of the molar extinction coefficient if the A-term dominates but will be linearly proportional if the B-term is controlling.[41]

Over the last twenty years we have been pioneering the development of UV resonance Raman spectroscopy for

Received 30 November 2009; accepted 4 February 2010.
* Author to whom correspondence should be sent. E-mail: asher@pitt.edu.

0003-7028/10/6404-0425$2.00/0

numerous applications, especially biological applications.[42–47] In the work presented here we have extended our UV Raman studies to explosive molecules and measured the deep UV Raman cross-sections of several explosives such as trinitrotoluene (TNT), pentaerythritol tetranitrate (PETN), cyclotrimethylene-trinitramine (RDX), the chemically related nitroamine explosive HMX, and ammonium nitrate. We find that deep UV Raman cross-sections for these explosives are roughly three orders of magnitude larger than those for 532 nm excitation. These increased Raman cross-sections enable parts-per-billion (ppb) detection level limits for these molecules, indicating promise for the utility of deep UV resonance Raman spectroscopy for stand-off detection of explosives.

EXPERIMENTAL

Materials. Small quantities of the explosives TNT, PETN, RDX, and HMX were a gift from the Federal Aviation Association to the University of Pittsburgh and were used as received. Ammonium nitrate (NH_4NO_3) was purchased from EM Industries, Inc. (Gibbstown, NJ, an associate of Merck) and used as received. Acetonitrile (ACN), HPLC grade, was purchased from EMD Chemicals, Inc. (Gibbstown, NJ) and used as received.

Ultraviolet Absorption Measurements. Absorption spectra at 200–400 nm of the explosives in solution were measured by using a Cary 5000 UV-VIS-NIR spectrophotometer (Varian, Inc.), operated in a double-beam mode. Absorption spectra of TNT, HMX, RDX, PETN, and NH_4NO_3 were measured in a 1 mm path length quartz cell at 0.1 mg/mL sample concentrations. ACN was used as a solvent for TNT, HMX, RDX, and PETN. Pure water was used for NH_4NO_3.

229 nm Ultraviolet Raman Instrumentation. The UV Raman instrument was described in detail elsewhere.[48–50] An Innova 300 FReD Ar^+ laser (Coherent, Inc.) was used to generate continuous wave (cw) 229 nm light.[50] The laser beam was focused onto the sample by using a 1 in. diameter fused silica lens with a focal length of 15 cm. We used a ~150° backscattering geometry. The UV Raman scattered light was dispersed by using a SPEX 1877 Triplemate spectrometer modified for deep UV Raman measurements.[48] We detected the UV Raman spectra using a Roper Scientific Spec-10:400B charge-coupled device (CCD) camera.

266 nm Ultraviolet Raman Instrumentation. The 266 nm UV Raman setup we used is essentially similar to the 229 nm UV Raman setup described above. The only difference is that we used the fourth harmonic of a Nd:YAG Infinity laser to provide a source of 266 nm light.

229 nm Ultraviolet Raman Measurements of Explosives in Solution Phase. Fifteen to twenty-five milliliters (15–25 mL) of each solution of explosives was circulated in an open stream flow system (diameter = 0.6 mm) described earlier.[48,49] The continuous sample flow prevents sample depletion and the contribution of excited states and degradation products, which could result from photochemical and photothermal degradation processes and photoproducts.[51,52] To detect the possible occurrence of sample degradation and solvent evaporation, we consecutively collected three spectra of each sample solution with 3–5 min accumulation times for each. We found that essentially no UV Raman spectral variations occur between three consecutive spectra of TNT, PETN, HMX, RDX, and NH_4NO_3 in these solution measurements.

TNT, RDX, and HMX were studied at concentrations of 0.54 to 5.2 mg/mL in neat ACN, while the PETN solution concentrations were in the range of 8.9 to 19 mg/mL. The ACN Raman bands were used as internal and frequency standards to determine the 229 nm absolute Raman cross-sections of the explosives by using the methods of Dudik et al.[53] We neglected to correct the raw spectra displayed for self-absorption or the wavelength dependence of the spectrometer efficiency; the analyte bands are quite close to those of the solvent internal standard bands and the absorption spectra are broad. Further, the entire measured Raman spectral wavelength range is quite small in the UV.

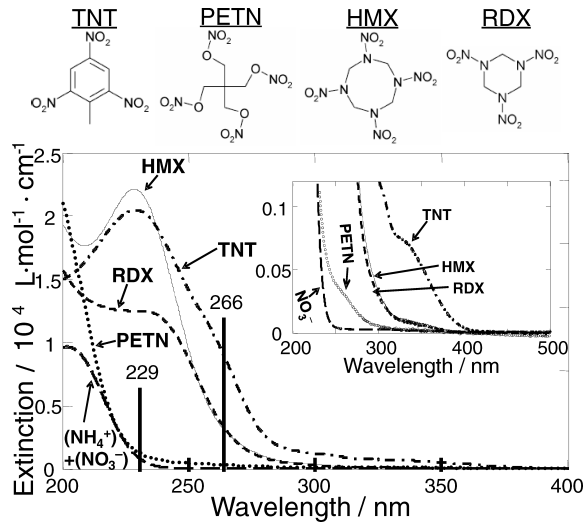

FIG. 1. Chemical structures and molar absorptivities of TNT, HMX, RDX, and PETN in acetonitrile, and NH_4NO_3 in water. Spectra were measured at sample concentrations of 0.1 mg/mL in a 1 mm quartz cell. Inset: Expanded absorbance scale.

We prepared NH_4NO_3 solutions at concentrations between 1.6 and 23.7 mg/mL in 77% ACN:23% water solutions. Water was used to dissolve the NH_4NO_3, while ACN was used as an internal intensity and frequency standard to determine the 229 nm absolute Raman cross-sections.[53]

266 nm Ultraviolet Raman Measurements of Solution TNT. In addition to 229 nm solution studies, we also measured 266 nm UV Raman spectra from solutions of TNT in ACN. The measurement strategy was similar to that used for the 229 nm excitation studies. The only difference is that instead of an open-stream flow cell we used a 5 mm quartz cell. To reduce possible TNT degradation we utilized a rotating small Teflon®-coated magnetic stir-bar placed inside the quartz cell.

Deep Ultraviolet Raman Measurements of Solid Explosives. Deep UV resonance Raman cross-section measurements of solid explosives require the solid sample to be dispersed as very small particles within a transparent medium containing an internal intensity standard. Accurate measurements not biased by self-absorption require particles sufficiently small that they do not significantly attenuate the excitation or Raman scattered light as it propagates through the particles. The appropriate particle size can be very small. For example, for TNT excited at ~266 nm, Fig. 1 indicates that in solution $\varepsilon \sim 10^4\ M^{-1}\ cm^{-1}$. Given a density of ~1.7 gm/Mole, a solid TNT thickness of 10 nm would show an absorbance of ~0.1. Thus, we require TNT particle diameters $\leq$10 nm. We are working to develop a method to prepare such small particles.

We measured the 266 nm resonance Raman spectra of ~10

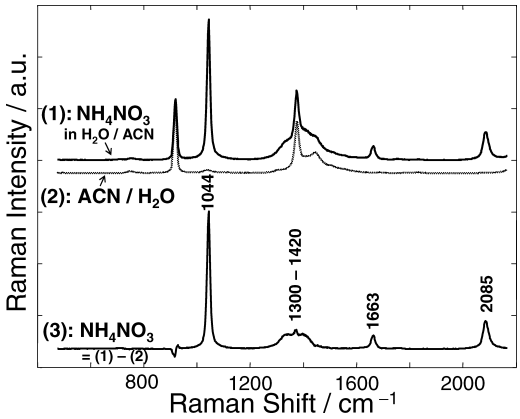

FIG. 2. 229 nm UV Raman spectra of NH_4NO_3. (*1*) 1.6 mg/mL NH_4NO_3 in 77% ACN/23% H_2O mixture, (*2*) ACN/water spectrum, (3) pure NH_4NO_3 spectrum, with the ACN/water spectrum numerically removed.

μm average particle size solid TNT suspended within water, within which it is insoluble, in order to compare the solid TNT spectra to that dissolved in solution. This TNT particle dispersion was placed into a 5 mm fused silica cuvette, which contained a small Teflon-coated magnetic stir-bar. To ensure a homogeneous distribution of the solid explosive particles we aggressively stirred the suspension using a small Teflon-covered magnetic stirbar. This rapid stirring prevents sample bleaching and laser heating, which can lead to sample degradation and spectral contributions of excited states or sample degradation products.

The previous measurements of solid explosive Raman cross-sections of Nagli et al.,[35] who utilized a thick external standard sample of KNO_3 and a separate thick pure explosive sample, must be strongly biased by self-absorption because they did not account for the different absorption and scattering of the excitation and Raman scattered light from the explosive solid-state sample and the solid external standard sample. Obviously there will be different and unknown penetration depths of the excitation beam into these samples. Nagli et al.[35] also incorrectly assumed identical cross-sections for NO_3^- in aqueous solutions and in the solid state. The resonance Raman cross-sections could radically differ between solid and solution phases.

RESULTS AND DISCUSSION

Absorption Spectra of NH_4NO_3, TNT, HMX, RDX, and PETN. Figure 1 shows the chemical structures and the 200–400 nm absorption spectra of TNT, HMX, RDX, and PETN in ACN, as well as the absorption spectrum of NH_4NO_3 in water. As expected, NH_4NO_3 and PETN show absorption maxima at ~200 nm, with 200 nm molar extinction coefficients of 0.96×10^4 $L \cdot mol^{-1} \cdot cm^{-1}$ and 2.1×10^4 $L \cdot mol^{-1} \cdot cm^{-1}$, respectively. PETN shows an additional weak absorption shoulder at ~260 nm.[54]

The ~200 nm NO_3^- absorption can be assigned to a NO_3^- group $\pi \rightarrow \pi^*$ transition.[55] The ~194 nm PETN absorption band was previously assigned to a $\pi \rightarrow \pi^*$ transition based upon molecular orbital (MO) calculations of the $C_2H_5ONO_2$ molecule. The MO calculations by Mullen and Orloff indicate a $\pi \rightarrow \pi^*$ transition of the $-NO_2$ group with a large contribution from an intramolecular charge transfer transition involving electron density transfer from the C_2H_5O atoms to the $-NO_2$ group.[54]

The 200 nm extinction coefficient per NO_3 group[54] of NH_4NO_3 is approximately twice that for the $-CH_2-NO_3$ group of PETN (Fig. 1). Presumably, this results from the fact that the PETN NO_3 groups are bound to methylenes. This structural difference also results in the additional PETN weak absorption feature at ~260 nm (Fig. 1 inset), which has been assigned to an $n \rightarrow \pi^*$ electronic transition of the $-NO_3$ group.[54] A weak $n \rightarrow \pi^*$ absorption can also be observed at very high NO_3^- concentrations.[55]

The HMX and RDX absorption spectra are more complex than those of PETN and NH_4NO_3. There are at least two electronic transitions contributing to the HMX and RDX $-N-NO_2$ absorption in the 200–250 nm region, one with a maximum below 200 nm, while the other is centered at ~230 nm. The latter transition mainly originates from a $\pi \rightarrow \pi^*$ transition.[56,57] Stals et al.[57] indicate that the assignment of the ~200 nm broad band is complicated by the "intimate mixing" of σ, π, σ^*, π^*, and n orbitals, which are of similar energies.

Whatever the case, the absorption per $-N-NO_2$ group for HMX is approximately 25% more than that for RDX, indicating electronic structure differences. Our 229 nm resonance Raman data (see below) confirm that the RDX and HMX electronic transitions are delocalized, providing resonance enhancement of numerous vibrational modes. In addition, there are also very weak and broad RDX and HMX absorption features between 280 and 380 nm (Fig. 1 inset).

In contrast to our solution RDX and HMX absorption spectra, Stals noted that crystalline RDX shows an additional absorption at ~340 nm[58] that is not evident in solution RDX absorption spectra. Also, Stals suggested that RDX and HMX form charge transfer complexes upon crystallization.[58]

TNT shows at least three electronic transitions in the 200–400 nm spectral region. The highest molar absorptivity band occurs at ~229 nm. A shoulder is evident at ~260 nm with a weak broad feature occurring between 280 and 340 nm. The assignments of these transitions are complex but provide insight into the enhancements.[56,59,60]

The absorption spectra of all of these explosive molecules show that Raman spectra of these compounds excited by using >280 nm excitation should show little or no resonance Raman enhancement. Since resonance Raman enhancement roughly scales with the square of the molar extinction coefficient,[41] we expect that ~229 nm excitation will result in the strongest UV Raman spectra for TNT and HMX, whereas the 229 nm excited RDX Raman spectra should be of intermediate intensity and the spectra of NH_4NO_3 and PETN will be significantly weaker.

One of the goals of the study here is to determine the conditions for obtaining the optimal signal-to-noise ratio for stand-off detection of explosives. A complication of UV Raman measurements is that low duty cycle pulsed laser excitation can give rise to nonlinear optical responses such as Raman saturation and excited-state formation and sample degradation.[51] Thus, we here use cw laser excitation in flowing open-liquid stream samples and stirred solid dispersions.

229 nm Ultraviolet Raman Spectra of NH_4NO_3 in 23% Water in ACN Solution. Figure 2 compares the 229 nm UV Raman spectrum of 1.6 mg/mL NH_4NO_3 in an ACN solution containing 23% water, the Raman spectrum of the ACN/water solution, and their difference spectrum. The ACN contribution was removed by normalizing to the ~918 cm^{-1} and 2249 cm^{-1}

TABLE I. Absolute Raman cross-sections at 229 nm and detection limits of explosives in solution phase.

Explosive species	Estimated 229 nm Raman detection limit	229 nm Raman bands, cm^{-1}	229 nm absolute Raman cross-sections/$10^{-26}cm^2$/(molc sr)
TNT (in ACN)	100 ppb (ACN)	826	4.0
		1170	2.2
		1208	5.3
		1361	**54.6**
		1624	**25.4**
			Σ_{TNT} (cross-section sum): 91.5, ε_{229}^2: 4.2 × 10^8
PETN (in ACN)	2200 ppb (ACN)	**872**	**1.1**
		1279	0.83
		1295	**1.6**
		1511	0.71
		1658	**1.1**
			Σ_{PETN}: 5.34, ε_{229}^2: 1.9 × 10^6
NH_4NO_3 (in CAN/H_2O)	250 ppb (water)	**1044**	**7.4**
		1325	2.9
		1372	0.65
		1400	2.1
		1663	1.1
		2085	3.1
			Σ_{NH4NO3}: 17.3, ε_{229}^2: 9.9 × 10^5
HMX (in ACN)	160 ppb (ACN)	758	1.4
		840	5.2
		879	**12.0**
		941	**33.1**
		1031	**13**
		1079	5.0
		1139	6.4
		1182	**7.8**
		1221	**9.9**
		1261	**13.7**
		1329	**14.6**
		1365	1.3
		1521	**5.0**
		1580	**9.7**
			Σ_{HMX}: 140, ε_{229}^2: 4.9 × 10^8
RDX (in ACN)	850 ppb (ACN)	758	1.4
		794	0.4
		852	2.2
		885	2.5
		924	0.9
		948	5.8
		1025	**6.3**
		1218	5.4
		1267	**5.8**
		1335	2.5
		1381	**5.5**
		1458	3.4
		1517	1.5
		1589	4.0
			Σ_{RDX}: 48, ε_{229}^2: 1.6 × 10^8

ACN bands. The water Raman bands are of negligible intensity.

The NH_4NO_3 229 nm Raman spectrum (Fig. 2, bottom) is essentially identical to that reported by Ianoul et al. for NO_3^- ions in water.[61] The contribution from NH_4^+ is negligible. For example, even a 100 mg/mL NH_4Cl spectrum shows essentially no NH_4^+ UV Raman bands (not shown). Thus, all the 229 nm Raman bands of NH_4NO_3 originate from NO_3^-.

The normal modes of nitrate ions in water solutions were thoroughly studied both experimentally and theoretically.[62–67] Summarizing, the ~1044 cm^{-1} band is assigned to a totally symmetric NO_3^- stretching vibration (ν_1, A'_1). The ~1300–1420 cm^{-1} bands are assigned to the asymmetric NO_3^- stretching (ν_3, E') coupled to water motion(s). The ~1663 cm^{-1} band is assigned to an overtone of the out-of-plane

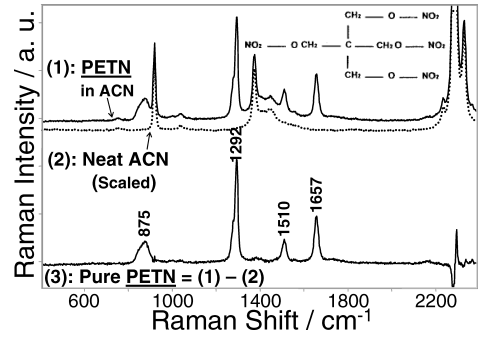

FIG. 3. 229 nm UV Raman spectra of PETN, not corrected for self-absorption. (*1*) pure ACN, (*2*) 18.9 mg/mL PETN in ACN, (*3*) pure PETN spectrum, with ACN contribution numerically removed.

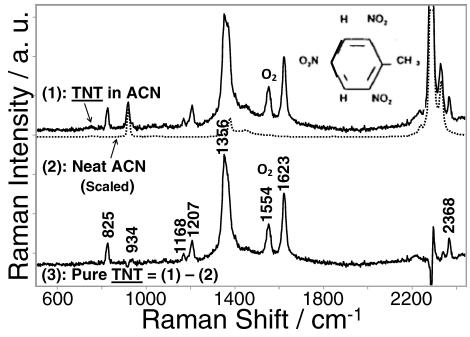

FIG. 4. 229 nm UV Raman spectra of TNT not corrected for self-absorption. (*1*) 2 mg/mL TNT in ACN, (*2*) pure ACN, (*3*) pure TNT spectrum, with ACN contribution numerically removed. The 1554 cm^{-1} band derives from oxygen in the air.

deformation ($2\cdot\nu_2$, A''_2), and the ~2076 cm^{-1} band is assigned to the overtone of the ~1040 cm^{-1} NO_3^- symmetric stretch band ($2\cdot\nu_1$). The barely visible ~723 cm^{-1} feature can be assigned to NO_3^- in-plane bending (ν_4, E'), which is Raman active for the D_{3h} symmetry group. As expected, the ~830 cm^{-1} out-of-plane deformation band (ν_2, A''_2) is not observed, since it is not Raman active in the D_{3h} symmetry group.[62] Although the ν_2 vibration fundamental (~830 cm^{-1}) is not observed, its overtone, $2\cdot\nu_2$ (1663 cm^{-1}), is strong (Fig. 2) because the overtone contains the totally symmetric representation.

As shown earlier by Ianoul et al.,[61] we easily obtained a 229 nm ~14 μM (~250 ppb) detection limit for NO_3^- ions in H_2O with only 10 min spectral accumulations. This is in spite of the modest <5% efficiency of the Triplemate Raman spectrometer utilized for these measurements.[48] Table I lists the calculated Raman cross-sections of the NO_3^- Raman bands.

229 nm Ultraviolet Raman Spectra of PETN in ACN. Figure 3 shows the 229 nm UV Raman spectrum of 18.9 mg/mL PETN in ACN, pure ACN, and the difference spectrum with the ACN contribution numerically removed by using the ~918 cm^{-1} and 2249 cm^{-1} ACN bands as an internal subtraction standard. This 229 nm excited pure PETN preresonant Raman spectrum (Fig. 3, bottom) is similar to 488 nm excited "solution-phase" Raman spectrum of PETN in acetone-d_6 reported by Gruzdkov et al.,[68] as well as to other normal Raman spectra of PETN crystals.[7,11,13,15,17,18,35,69,71]

The PETN normal modes were studied in detail.[70,71] The broad ~875 cm^{-1} medium-weak band (Fig. 3, bottom) is assigned to O–N stretching with some contribution from C–C stretching. The strong ~1292 cm^{-1} band with a ~1279 cm^{-1} shoulder mainly originates from the $-NO_2$ symmetric stretch with a minor contribution from CH bending, CH_2 wagging, and C_5 skeletal vibrations. The medium-weak ~1510 cm^{-1} band can be assigned to CH_2 scissoring, while the medium intensity ~1657 cm^{-1} band is dominated by the $-NO_2$ asymmetric stretch vibration.

We can estimate the PETN 229 nm Raman detection limit, RDL_{229}, from the PETN calculated Raman cross-sections by using Eq. 1:

$$RDL_{229}(PETN) = RDL_{229}(NH_4NO_3) \times \sigma_m(NH_4NO_3)/\sigma_m(PETN) \quad (1)$$

where $RDL_{229}(PETN)$ and $RDL_{229}(NH_4NO_3)$ are the 229 nm Raman detection limits for PETN and NH_4NO_3, respectively; $\sigma_m(NH_4NO_3)$ and $\sigma_m(PETN)$ (shown in Table I) are cross-sections of the strongest 1044 cm^{-1} and (1295 cm^{-1} and 1279 cm^{-1} shoulder) Raman bands of NH_4NO_3 and PETN, respectively. We estimate that the PETN 229 nm Raman detection limit in ACN is ~43 μM or 2.2 ppm. If PETN were soluble in water, its detection limit would be ~0.76 ppm (Table I). This calculated detection limit utilizes the measured fact that spectrometer efficiency is essentially constant over the Raman spectral interval with 229 nm excitation and that the background intensity does not vary between compounds; shot noise from background is constant. This is a good assumption for UV excitation below 260 nm since fluorescence does not occur in this spectral region for condensed-phase samples.[40]

229 nm Ultraviolet Raman Spectra of TNT in ACN. Figure 4 shows the 229 nm UV Raman spectrum of a 2 mg/mL solution of TNT in ACN, pure ACN, and the pure TNT spectrum with the ACN contribution numerically removed. The ACN contribution was removed using the ~918 cm^{-1} and 2249 cm^{-1} ACN bands. The Fig. 4 pure TNT spectrum is essentially identical to previously reported spectra.[7,14–16,18,35,69,72–74] According to the TNT vibrational studies of Clarkson et al.,[75] the medium-weak ~825 cm^{-1} TNT band can be assigned to the NO_2 scissoring vibration. The weak ~1168 cm^{-1} band can be assigned to a vibration involving a combination of C–C ring in-plane trigonal bending with C–N and maybe C–CH_3 stretching. The medium-weak ~1207 cm^{-1} band derives from a totally symmetric aromatic "ring-breathing" mode. The strongest ~1356 cm^{-1} band derives from NO_2 symmetric stretching coupled to CN stretching. The ~1554 cm^{-1} band originates from atmospheric oxygen (O_2 stretch). The medium-strong ~1623 cm^{-1} band originates from asymmetric NO_2 stretching coupled to aromatic ring stretching.

Using Eq. 1 we estimate a TNT in ACN (water) detection limit of ~1.9 μM or 100 ppb (0.6 μM or ~34 ppb).

229 nm Ultraviolet Raman Spectra of HMX in ACN. Figure 5 shows 229 nm UV Raman spectra of 2.1 mg/mL HMX in ACN, pure ACN, and the pure HMX spectrum obtained by numerically removing the ACN contribution by spectrally subtracting the 2249 cm^{-1} ACN band intensity. The resulting pure resonance Raman HMX spectrum (Fig. 5, bottom) is similar to previously reported HMX Raman spectra.[14,15,18,72,76–79]

The 229 nm HMX Raman spectrum (Fig. 5) is spectrally rich and contains at least 16 resolved bands. We tentatively assign the HMX Raman bands using the theoretical studies of Brand et al.[80] and Zhu et al.[81] of the crystal HMX normal modes. The Fig. 5 HMX Raman spectrum is dominated by the 879 (ν_s-NNC_2 with ONO-b), 940 (ν_{as}-CNN with some CH_2 rocking), 1219 cm^{-1} (ν_{as}-NC_2), and 1261 cm^{-1} (ν_s-NO_2) bands. Other weaker bands are located at 758 cm^{-1} (NO_2 wagging vibration), 838 cm^{-1} (ν_s-NC_2), 908 cm^{-1} (ONO bending with ν_s-NNC_2), 1026 cm^{-1} (ν_s-NNC_2), 1072 (ν_s-NNC_2 with ONO-b), 1142 cm^{-1} (ν_{as}-NC_2 or ν_{as}-CNN with some CH_2 rocking (depending on whether the HMX symmetry group is C_i or C_{2V}), 1181 cm^{-1} (ν_{as}-NC_2), 1328 cm^{-1} (ν_s-NO_2 with some CH_2 twist about the NN bond), 1519 cm^{-1} (ν_{as}-NO_2), 1556 cm^{-1} (ν_{as}-NO_2), and 1576 cm^{-1} (ν_{as}-NO_2).

We estimate the 229 nm HMX in ACN detection limit to be 3.2 μM or 160 ppb. If HMX were soluble in water, then its detection limit there would be ~56 ppb.

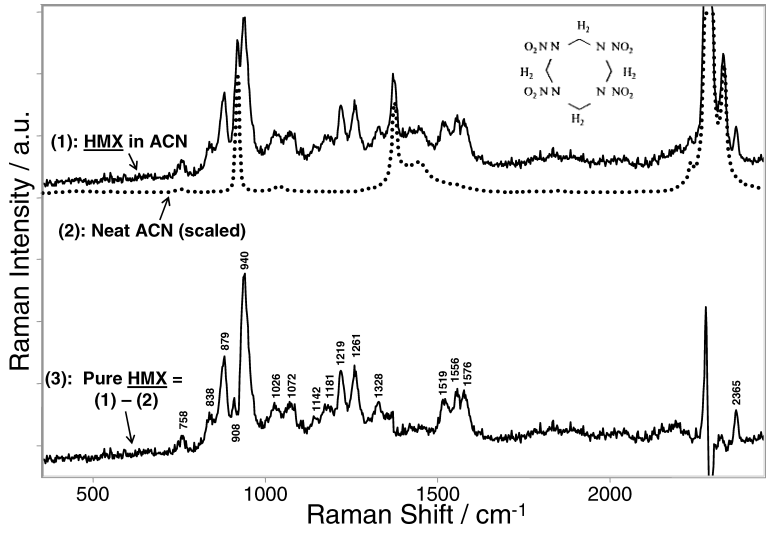

FIG. 5. 229 nm UV Raman spectra of HMX not corrected for self-absorption. (*1*) 1 mg/mL HMX in ACN, (*2*) pure ACN spectrum, (*3*) pure HMX spectrum, with ACN contribution numerically removed.

229 nm Ultraviolet Raman Spectra of RDX in ACN. Figure 6 shows the 229 nm UV Raman spectra of 1.33 mg/mL RDX in ACN, pure ACN, and pure RDX with the ACN contribution numerically removed by spectrally subtracting the 2249 cm^{-1} ACN band. The pure RDX 229 nm Raman spectrum is similar to most of the RDX Raman spectra previously reported.[19,20,54,67,76,78,82–86] The only exception is the 266 nm UV Raman spectrum of solid RDX reported by Nagli et al.;[35] Nagli et al.'s RDX may have degraded upon exposure to the high intensity 266 nm excitation light.

The pure RDX 229 nm Raman spectrum is very rich. We can assign its Raman bands from the normal mode studies of Dreger and Gupta.[21] The Fig. 6 RDX spectrum consists of at least 18 resolved bands: the 759 cm^{-1} (ring bending with NO_2 scissoring), 795 cm^{-1} (CN stretch and NO_2 scissoring), 851 cm^{-1} (NN stretch + NO_2 axial scissoring), 885 cm^{-1} (mainly CN stretch), 924 cm^{-1} (CH_2 rocking or combination), 950 cm^{-1} (NN stretch), 1024 cm^{-1} (NC stretch with some CH_2 rocking), 1215 cm^{-1} (NC stretching), 1268 cm^{-1} (NN stretching and ONO stretching, maybe with CH_2 twist), 1315 cm^{-1} (NN stretching and CH_2 twist), 1341 cm^{-1} (CH_2 wag or combination), 1378 cm^{-1} (CH_2 twisting), 1458 cm^{-1} (CH_2 scissoring), 1514 cm^{-1} (CH_2 scissoring or combination), 1559 cm^{-1} (ONO equatorial stretching), and 1585 cm^{-1} (ONO axial stretching).

We estimate the 229 nm "RDX in ACN" detection limit to be ~16.4 μmol or ~850 ppb. If RDX were soluble in water, then its UV Raman detection limit there would be ~300 ppb.

229 nm Absolute Raman Cross-Sections of Solution Phase TNT, PETN, HMX, RDX, and NH_4NO_3. Although there are a number of UV Raman studies of explosive molecules[35,74,87–89] there are few Raman cross-section determinations, especially in the deep UV.[34,35,74,87–96] Further, to our knowledge there are no reliable deep UV Raman cross-section data for explosives in the solid state.

Table I lists our measured 229 nm absolute Raman cross-

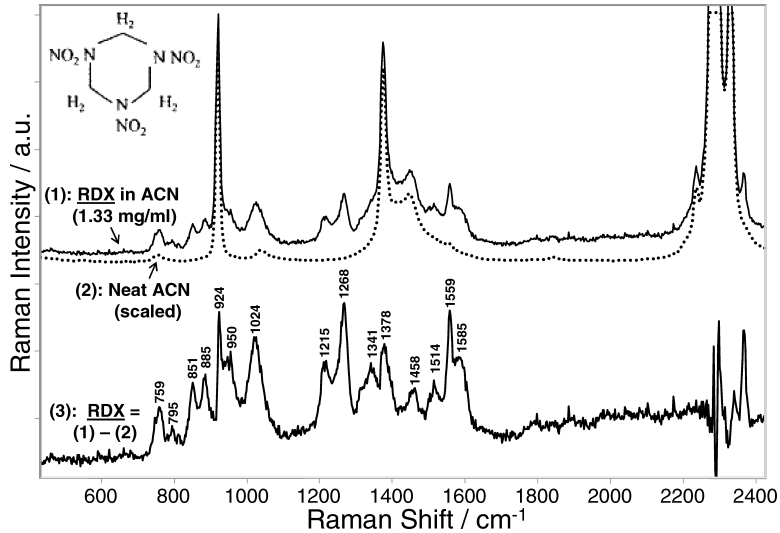

FIG. 6. 229 nm UV Raman spectra of RDX not corrected for self-absorption. (*1*) 1.33 mg/mL "RDX in ACN" spectrum, (*2*) pure ACN spectrum, (*3*) pure RDX spectrum, with the ACN contribution numerically removed.

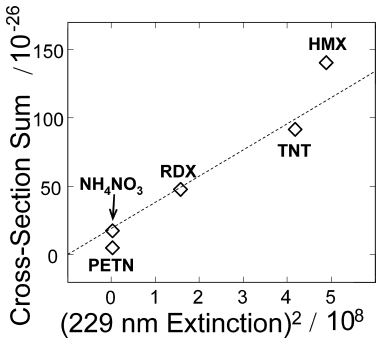

FIG. 7. Correlation between the sum of the 229 nm Raman cross-sections and the square of 229 nm molar extinction coefficients for TNT, HMX, RDX, NH_4NO_3, and PETN.

sections and detection limits for TNT, PETN, RDX, HMX, and NH_4NO_3 in solution. From the Albrecht A term approximation of the Raman cross-section enhancement for a single resonance electronic transition, we expect that the Raman cross-sections will roughly scale with the square of the molar absorptivity.[41] Table I and Fig. 7 demonstrate an excellent correlation between the sum of all the UV resonance Raman band cross-sections, Σ_{229}, and the square of the 229 nm molar absorptivity of each compound.

Comparison Between 229 nm Absolute Raman Cross-Sections and Previous Measurements at Longer Wavelength Excitation. We find ~100-fold larger 229 nm Raman solution cross-sections (Table I) compared to the 266 nm Raman solid-state sample cross-sections reported by Nagli et al.[35] This is a surprisingly large difference, especially for those molecules with similar absorptivities at these wavelengths. Although, this difference could occur if the Raman excitation profiles were strongly wavelength dependent, it would be unusual for typical organic molecules, which should have large absorption homogeneous bandwidths. We believe the most likely explanation is that the Nagli et al. external standard measurement is downwardly biased because it does not account for the different penetration depths of the excitation through the explosive and through the KNO_3, which results from sample absorption and scattering. The explosives have the larger absorption, which biases the measurement towards smaller Raman cross-sections. In addition, it is incorrect to assume identical Raman cross-sections for solution and solid NH_4NO_3 samples.

266 nm Ultraviolet Raman Spectra of Solid versus Solution TNT. Figure 8 compares the 266 nm Raman spectrum of solid TNT suspended in water to the solution spectrum of TNT in ACN (with water and ACN contributions numerically removed). Both spectra were measured in a 5 mm path length Quartz cell, stirred with a rotating small magnetic stirrer. This study demonstrates that the solid and solution state give rise to similar spectra in the fingerprint region but with somewhat higher solid-state intensities in the low frequency region. The important point is that the spectra are similarly diagnostic of the TNT molecular species.

We intend to determine the resonance Raman cross-sections of explosives in solid-state samples. We require samples for which the excitation and Raman scattered light is not significantly attenuated as it traverses the sample particles. We are working towards dispersing the explosives more finely within transparent internal standard matrices.

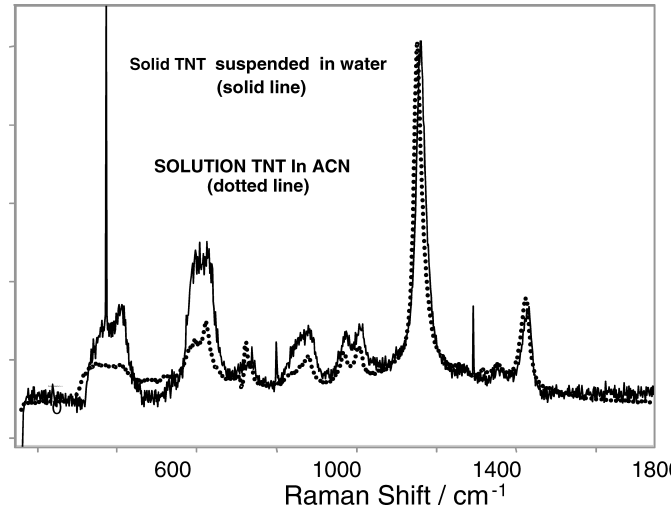

FIG. 8. 266 nm Raman spectra of 20 mg/mL solid TNT suspended in water versus 1 mg/mL solution of TNT in ACN. Water and ACN contributions were numerically removed. TNT suspension in water was aggressively mixed using a magnetic stirrer placed inside the 5 mm quartz cell to obtain a homogeneous suspension.

CONCLUSION

We measured for the first time 229 nm deep UV Raman cross-sections of TNT, PETN, HMX, RDX, and NH_4NO_3 in solution and compared solid-state and solution-state 266 nm Raman spectra of TNT. Our measured UV Raman cross-sections are much greater than the previously reported nonresonant visible and near-infrared spectral Raman measurements. The 229 nm UV Raman excitation detection limits for these explosives in solution are estimated to be ~100 ppb levels. We conclude that deep UV Raman spectroscopy is a very promising tool for explosive detection and has promise for use in stand-off detection.

ACKNOWLEDGMENTS

We acknowledge partial funding of this work by the Department of Homeland Security Science and Technology Directorate under contract number HSHQDC-09-C-00159, and partial funding from the University of Pittsburgh.

1. D. S. Moore, Rev. Sci. Instrum. **75,** 2499 (2004).
2. E. M. A. Ali, H. G. M. Edwards, M. D. Hargreaves, and I. J. Scowen, J. Raman Spectrosc. **40,** 144 (2009).
3. E. D. Emmons, A. Tripathi, J. A. Guicheteau, S. D. Christesen, and A. W. Fountain III, Appl. Spectrosc. **63,** 1197 (2009).
4. F. C. DeLucia, Jr., R. S. Harmon, K. L. McNesby, R. J. Winkel, Jr., and A. W. Miziolek, Appl. Opt. **42,** 6148 (2003).
5. F. C. DeLucia, Jr., J. L. Gottfried, C. A. Munson, and A. W. Miziolek, Appl. Opt. **47,** G112 (2008).
6. L. C. Pacheco-Londono, W. Ortiz-Rivera, O. M. Primera-Pedrozo, and S. P. Hernandez-Rivera, Anal. Bioanal. Chem. **395,** 323 (2009).
7. J. C. Carter, S. M. Angel, M. Lawrence-Snyder, J. Scaffidi, R. E. Whipple, and J. G. Reynolds, Appl. Spectrosc. **59,** 769 (2005).
8. A. Pettersson, I. Johansson, S. Wallin, M. Nordberg, and H. Ostmark, Propellants Explos. Pyrotech. **34,** 297 (2009).
9. I. R. Lewis, N. W. Daniel, Jr., N. C. Chaffin, P. R. Griffiths, and M. W. Tungol, Spectrochim. Acta, Part A **51,** 1985 (1995).
10. D. Sulzle and P. Klaeboe, Acta Chem. Scand. A **42,** 165 (1988).
11. N. F. Fell, J. M. Widder, S. V. Medlin, J. B. Morris, R. A. Pesce-Rodriguez, and K. L. McNesby, J. Raman Spectrosc. **27,** 97 (1996).
12. N. W. Daniel, Jr., I. R. Lewis, and P. R. Griffiths, Appl. Spectrosc. **51,** 1868 (1997).
13. I. R. Lewis, N. W. Daniel, Jr., and P. R. Griffiths, Appl. Spectrosc. **51,** 1854 (1997).
14. K. L. McNesby and C. S. Coffey, J. Phys. Chem. B **101,** 3097 (1997).

15. M. L. Lewis, I. R. Lewis, and P. R. Griffiths, Appl. Spectrosc. **58,** 420 (2004).
16. M. L. Lewis, I. R. Lewis, and P. R. Griffiths, Vib. Spectrosc. **38,** 17 (2005).
17. K. E. Lipinska-Kalita, M. G. Pravica, and M. Nicol, J. Phys. Chem. B **109,** 19223 (2005).
18. S. D. McGrane, J. Barber, and J. Quenneville, J. Phys. Chem. A **109,** 9919 (2005).
19. J. J. Haycraft, L. L. Stevens, and C. J. Eckhardt, J. Appl. Phys. **100,** 053508 (2006).
20. J. A. Ciezak, T. A. Jenkins, Z. Liu, and R. J. Hemley, J. Phys. Chem. A **111,** 59 (2007).
21. Z. A. Dreger and Y. M. Gupta, J. Phys. Chem. B **111,** 3893 (2007).
22. V. Vacque, N. Dupuy, B. Sombret, J. P. Huvenne, and P. Legrand, Appl. Spectrosc. **51,** 407 (1997).
23. F. T. Docherty, P. B. Monaghan, C. J. McHugh, D. Graham, W. E. Smith, and J. M. Cooper, IEEE Sens. J. **5,** 632 (2005).
24. L. L. Stevens, J. J. Haycraft, and C. J. Eckhardt, Cryst. Growth Design **5,** 2060 (2005).
25. K.-Y. Lee, D. S. Moore, B. W. Asay, and A. Llobet, J. Energetic Mater. **25,** 161 (2007).
26. D. S. Moore and K.-Y. Lee, J. Raman Spectrosc. **38,** 1221 (2007).
27. D. S. Moore and R. J. Scharff, Anal. Bioanal. Chem. **393,** 1571 (2009).
28. J. D. Santillan, C. D. Brown, and W. Jalenak, Proc. SPIE-Int. Soc. Opt. Eng. **6540,** 65400P (2007).
29. R. J. Stokes, W. E. Smith, B. Foulger, and C. Lewis, Proc. SPIE-Int. Soc. Opt. Eng. **7119,** 7119OI (2008).
30. Y. Fleger, L. Nagli, M. Gaft, and M. Rosenbluh, J. Lumin. **129,** 979 (2009).
31. D. S. Moore, Fresenius J. Anal. Chem. **369,** 393 (2001).
32. S. D. McGrane and A. P. Shreve, J. Chem. Phys. **119,** 5834 (2003).
33. J. Oxley, J. Smith, J. Brady, F. Dubnikova, R. Kosloff, L. Zeiri, and Y. Zeiri, Appl. Spectrosc. **62,** 906 (2008).
34. M. Gaft and L. Nagli, Opt. Mater. **30,** 1739 (2008).
35. L. Nagli, M. Gaft, Y. Fleger, and M. Rosenbluh, Opt. Mater. **30,** 1747 (2008).
36. P. Jander and R. Noll, Appl. Spectrosc. **63,** 559 (2009).
37. L. Nagli and M. Gaft, Proc. SPIE-Int. Soc. Opt. Eng. **6552,** 6552OZ (2007).
38. R. D. Waterbury, A. R. Ford, J. B. Rose, and E. L. Dottery, Proc. SPIE-Int. Soc. Opt. Eng. **7304,** 73041B (2009).
39. W. F. Hug, R. D. Reid, R. Bhartia, and A. L. Lane, Proc. SPIE-Int. Soc. Opt. Eng. **6954,** 6954OI (2008).
40. S. A. Asher and C. R. Johnson, Science (Washington, D.C.) **225,** 311 (1984).
41. R. J. H. Clark, "Resonance Raman Spectra of Inorganic Molecules and Ions", in *Advances in Infrared and Raman Spectroscopy,* R. J. H. Clark and R. E. Hester, Eds. (Heyden, London, 1975), vol. 1, p. 151.
42. S. A. Asher, Anal. Chem. **65,** 59A (1993).
43. S. A. Asher, Anal. Chem. **65,** 201A (1993).
44. S. Bykov, I. Lednev, A. Ianoul, A. Mikhonin, C. Munro, and S. A. Asher, Appl. Spectrosc. **59,** 1541 (2005).
45. B. Sharma, S. Bykov, and S. A. Asher, J. Phys. Chem. B **112,** 11762 (2008).
46. A. Mikhonin, S. Bykov, N. Myshakina, and S. A. Asher, J. Phys. Chem. B **110,** 1928 (2006).
47. S. A. Asher, in *Handbook of Vibrational Spectroscopy*, J. M. Chalmers and P. R. Griffiths, Eds. (John Wiley and Sons, New York, 2001), vol. 1, pp. 557–571.
48. S. Bykov, I. Lednev, A. Ianoul, A. Mikhonin, C. Munro, and S. A. Asher, Appl. Spectrosc. **59,** 1541 (2005).
49. I. K. Lednev, A. S. Karnoup, M. C. Sparrow, and S. A. Asher, J. Am. Chem. Soc. **121,** 8074 (1999).
50. S. A. Asher, R. W. Bormett, X. G. Chen, D. H. Lemmon, N. Cho, P. Peterson, M. Arrigoni, L. Spinelli, and J. Cannon, Appl. Spectrosc. **47,** 628 (1993).
51. C. R. Johnson, M. Ludwig, and S. A. Asher, J. Am. Chem. Soc. **108,** 905 (1986).
52. J. Teraoka, P. A. Harmon, and S. A. Asher, J. Am. Chem. Soc. **112,** 2892 (1990).
53. J. M. Dudik, C. R. Johnson, and S. A. Asher, J. Chem. Phys. **82,** 1732 (1985).
54. P. A. Mullen and M. K. Orloff, J. Phys. Chem. **77,** 910 (1973).
55. V. Tomisic, V. Butorac, J. Viher, and V. Simeon, J. Sol. Chem. **34,** 613 (2005).
56. J. Stals, C. G. Barraclough, and A. S. Buchanan, Trans. Faraday Soc. **65,** 904 (1969).
57. J. Stals, Aust. J. Chem. **22,** 2515 (1969).
58. J. Stals, Trans. Faraday Soc. **67,** 1739 (1971).
59. A. K. Chaudhary, A. M. Rudra, P. Kumbhakar, and G. C. Bhar, J. Appl. Spectrosc. **74,** 571 (2007).
60. T. Abe, Bull. Chem. Soc. Jpn. **32,** 339 (1959).
61. A. Ianoul, T. Coleman, and S. A. Asher, Anal. Chem. **74,** 1458 (2002)
62. M. R. Waterland and A. Myers-Kelley, J. Chem. Phys. **113,** 6760 (2000).
63. M. R. Waterland, D. Stockwell, and A. Myers-Kelley, J. Chem. Phys. **114,** 6249 (2001).
64. A. Tongraar, P. Tangkawanwanit, and B. M. Rode, J. Phys. Chem. A **110,** 12918 (2006).
65. H. Torii, J. Phys. Chem. A **106,** 1167 (2002).
66. C. Ebner, R. Sansone, and M. Probst, Int. J. Quantum Chem. **70,** 877 (1998).
67. D. E. Irish and A. R. Davis, Can. J. Chem. **46,** 943 (1968).
68. Y. A. Gruzdkov, Z. A. Dreger, and Y. M. Gupta, J. Phys. Chem. A **108,** 6216 (2004).
69. K. L. McNesby, J. E. Wolfe, J. B. Morris, and R. A. Pesce-Rodriquez, J. Raman Spectrosc. **25,** 75 (1994).
70. Y. A. Gruzdkov and Y. M. Gupta, J. Phys. Chem. A **105,** 6197 (2001).
71. W. F. Perger, J. Zhao, J. M. Winey, and Y. M. Gupta, Chem. Phys. Lett. **428,** 394 (2006).
72. G. Comanescu, C. K. Manka, J. Grun, S. Nikitin, and D. Zabetakis, Appl. Spectrosc. **62,** 833 (2008).
73. N. Gupta and R. Dahmani, Spectrochim. Acta, Part A **56,** 1453 (2000).
74. C. H. Munro, V. Pajcini, and S. A. Asher, Appl. Spectrosc. **51,** 1722 (1997).
75. J. Clarkson, W. E. Smith, D. N. Batchelder, D. A. Smith, and A. M. Coats, J. Mol. Struct. **648,** 203 (2003).
76. N. F. Fell, J. M. Widder, S. V. Medlin, R. A. Pesce-Rodriquez, and K. L. McNesby, Proc. Beijing Int. Symp. Pyrotech. Explos., 3rd **1995,** 124 (1995).
77. F. Goetz and T. B. Brill, J. Phys. Chem. **83,** 340 (1979).
78. K. Y. Lee and D. S. Moore, AIP Conf. Proc. **955** (Pt. 2, Shock Compression of Condensed Matter—2007, Part 2), 975 (2007).
79. D. S. Moore, K. Y. Lee, and S. I. Hagelberg, J. Energy Mater. **26,** 70 (2008).
80. H. V. Brand, R. L. Rabie, D. J. Funk, I. Diaz-Acosta, P. Pulay, and T. K. Lippert, J. Phys. Chem. B **106,** 10594 (2002).
81. W. Zhu, J. Xiao, G. Ji, F. Zhao, and H. Xiao, J. Phys. Chem. B **111,** 12715 (2007).
82. K. L. McNesbey, N. F. Fell, Jr., and J. A. Vanderhoff, Proc. SPIE-Int. Soc. Opt. Eng. **3082,** 121 (1997).
83. N. F. Fell, Jr., J. A. Vanderhoff, R. A. Pesce-Rodriguez, and K. L. McNesby, J. Raman Spectrosc. **29,** 165 (1998).
84. R. Infante-Castillo and S. P. Hernandez-Rivera, Proc. SPIE-Int. Soc. Opt. Eng. **6538,** 653825 (2007).
85. P. Torres, L. Mercado, I. Cotte, S. P. Hernandez, N. Mina, A. Santana, R. T. Chamberlain, R. Lareau, and M. E. Castro, J. Phys. Chem. B **108,** 8799 (2004).
86. S. Ye, K. Tonokura, and M. Koshi, Chem. Phys. **293,** 1 (2003).
87. S. R. Ahmad and V. G. Foster, Appl. Spectrosc. **52,** 70 (1998).
88. S. R. Ahmad and V. G. Foster, J. Raman Spectrosc. **31,** 1023 (2000).
89. H. S. Sands, I. P. Hayward, T. E. Kirkbride, R. Bennett, R. J. Lacey, and D. N. Batchelder, J. Forensic Sci. **43,** 509 (1998).
90. A. Blanco, L. C. Pacheco-Londono, A. J. Pena-Quevedo, and S. P. Hernandez-Rivera, Proc. SPIE-Int. Soc. Opt. Eng. **6217,** 621737 (2006).
91. A. Blanco, N. Mina, M. E. Castro, J. Castillo-Chara, and S. P. Hernandez-Rivera, Proc. SPIE-Int. Soc. Opt. Eng. **5794,** 1281 (2005).
92. R. J. Lacey, I. P. Hayward, H. S. Sands, and D. N. Batchelder, Proc. SPIE-Int. Soc. Opt. Eng. **2937,** 100 (1997).
93. A. G. Mercado, J. Janni, and B. Gilbert, Proc. SPIE-Int. Soc. Opt. Eng. **2511,** 142 (1995).
94. M. D. Ray and A. J. Sedlacek, Proc. SPIE-Int. Soc. Opt. Eng. **3707,** 138 (1999).
95. M. D. Ray, A. J. Sedlacek, and M. Wu, Rev. Sci. Instrum. **71,** 3485 (2000).
96. A. J. Sedlacek, M. D. Ray, and M. Wu, Trends Appl. Spectrosc. **5,** 19 (2004).